ChemComm

COMMUNICATION

View Article Online
View Journal | View Issue

Cite this: *Chem. Commun.*, 2024, **60**, 9789

Received 1st June 2024,
Accepted 25th July 2024

DOI: 10.1039/d4cc02676d

rsc.li/chemcomm

Rim-differentiated pillar[5]arene-modified surfaces for rapid PFOA/PFOS detection†

Tu-Nan Gao, [a] Zhen Yang, [ab] Jesse M. S. Goed, [ac] Han Zuilhof *[ad] and Fedor M. Miloserdov *[a]

A new rim-differentiated pillar[5]arene (RD-P5) has been synthesized and immobilized onto an Al_2O_3 surface for the rapid detection of perfluoroalkyl acids. This P5-Al_2O_3 surface provides a novel approach for measuring perfluorooctane sulfonic acid (PFOS) and perfluorooctanoic acid (PFOA) using contact angle measurements, with limits of detection down to 10 ng L^{-1}.

Per- and polyfluoroalkyl substances (PFAS), known as "forever chemicals", have emerged as a significant environmental concern worldwide due to their presence in air, water, and soil.[1,2] Toxicity studies have demonstrated that the accumulation of PFAS can lead to a variety of health issues.[3–5] The US Environmental Protection Agency (EPA) initially set the advisory safe limit for perfluorooctane sulfonic acid (PFOS) and perfluorooctanoic acid (PFOA) at 70 ng L^{-1} in 2016, and in 2023, lowered this to 4 ng L^{-1} for each of these chemicals. The updated safe limit (4 ng L^{-1}) presents a great challenge for PFAS detection. Due to the poor molar optical absorption coefficient of PFOA and PFOS, the gold standard detection method is liquid chromatography–mass spectrometry (LC-MS). Although LC-MS is sensitive and accurate, it has drawbacks such as lengthy measurements, requiring expensive equipment, and the need for well-trained analytical chemists for operation. Efforts have been made to develop a more facile and sensitive PFAS detection workflow.[6–8] Electrochemical techniques utilizing electrodes modified with molecularly imprinted polymers (MIP) or metal–organic frameworks (MOF) have shown promising results, achieving a limit of detection (LOD) as low as 1.7 ng L^{-1} for MIP-modified electrodes[9] and 1 ng L^{-1} for MOF-modified electrodes.[10] Fluorescence-based techniques can also reach LOD of 80 ng L^{-1} for PFOA and 350 ng L^{-1} for PFOS by using amplifying fluorescent polymers (AFP) as sensing element.[11] However, while being highly sensitive, both electrochemical and fluorescent techniques again require specific lab-based equipment for their implementation, such as an impedance analyzer or fluorescence spectrometer. This limitation restricts their applicability for on-site PFAS detection. On the other hand, colorimetry, which is convenient to use for on-site applications because of its integration with common smartphones, often exhibits a significantly lower sensitivity,[12] with typical LODs from 10 μg L^{-1} to 1 mg L^{-1}.[13–17]

While much research is focused on detecting PFAS through changes in either optical or electrochemical properties of probe materials, to the best of our knowledge no investigations have been conducted to detect PFAS by a change of surface contact angle. Contact angle changes can be easily measured on-site using smartphones, and such technology is already used in the detection of ctDNA or metal ions.[18,19] In a previous study, we developed a deca-ammonium-functionalized pillar[5]arenes (DAF-P5s) capable of binding to polyfluoroalkyl acids at a 1 : 10 host–guest ratio, and exhibiting high binding constants in aqueous environments of up to 10^6 M^{-1}.[20] Similarly, perfluorinated diacids ($HOOC–(CF_2)_nCOOH$) form pillar-like supramolecular structures that can reach macroscopic sizes, again displaying strong and unique interactions with PFAS.[21] This high affinity arises from the unique structure of DAF-P5s, which feature five tightly packed amine moieties capable of attaching five PFAS molecules per rim. This attachment leads to the formation of a stable local fluorous phase, resulting in the observed high binding constant. Herein, we report the synthesis of a dual-functionalized rim-differentiated pillar[5]arene RD-P5 and its immobilization on a surface for on-site detection of PFOA and PFOS at ng L^{-1} levels through a simple, near-instantaneous water contact measurement (Scheme 1).

The DAF-P5s that we previously successfully employed for PFAS binding are not suitable for direct immobilization onto a surface.[20] To introduce the unique property of DAF-P5s on a

[a] *Laboratory of Organic Chemistry, Wageningen University, Stippeneng 4, 6708WE Wageningen, The Netherlands. E-mail: fedor.miloserdov@wur.nl, han.zuilhof@wur.nl*
[b] *Imec within OnePlanet Research Center, Bronland 10, 6708 WH Wageningen, The Netherlands*
[c] *Wetsus, Oostergoweg 4, 8911 MA Leeuwarden, The Netherlands*
[d] *School of Pharmaceutical Science and Technology, Tianjin University, Weijin Road 92, 300072 Tianjin, China*

† Electronic supplementary information (ESI) available. CCDC 2359089. For ESI and crystallographic data in CIF or other electronic format see DOI: https://doi.org/10.1039/d4cc02676d

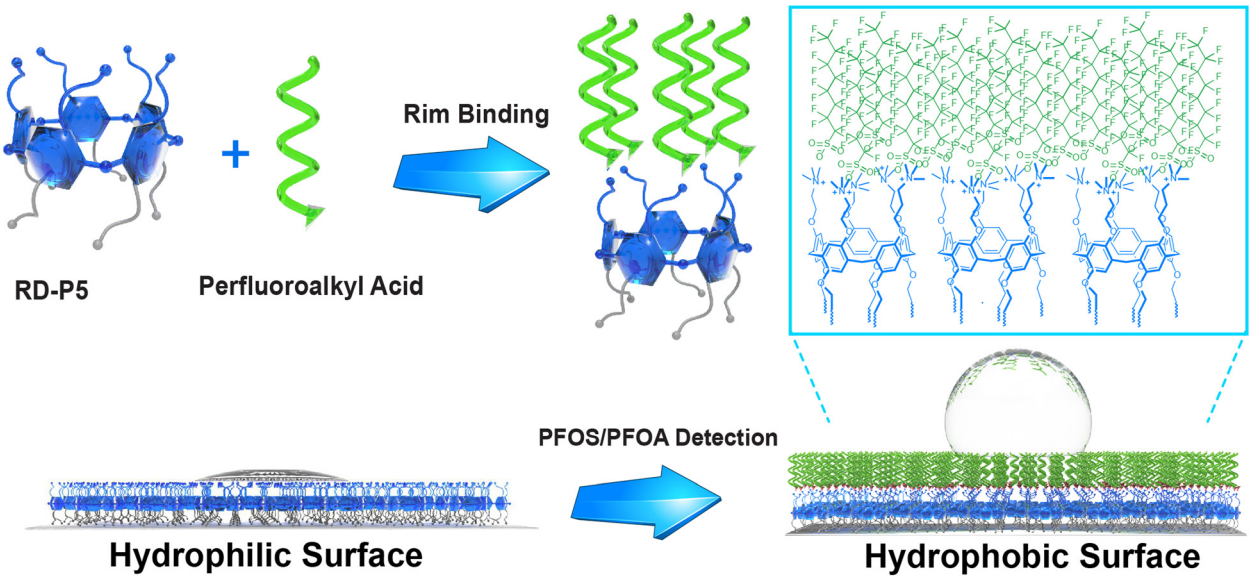

Scheme 1 RD-P5 **2**-modified surface for PFOA/PFOS detection.

surface, we designed rim-differentiated pillar[5]arene (RD-P5) **2**, bearing 5 alkyne moieties for surface immobilization on one rim and 5 positively charged trimethyl ammonium groups for PFAS binding on the other. Since statistical synthesis of RD-P5 is only very low yielding (typically $<5\%$),[22] our group previously developed the "pre-orientation" strategy,[23,24] that leads to $>50\%$ RD-P5 formation and concomitantly decent isolated yields. With this significant improvement, the synthesis of RD-P5s is no longer the bottleneck for their application. However, the number of papers employing RD-P5,[25–32] and particularly of RD-P5s with dual-functionalized rims, remains limited.[33–36]

We synthesized RD-P5 **1** following the "pre-oriented" strategy.[23] From the ^{1}H NMR spectra of crude product (Fig. S1, ESI†), the presence of P5 constitutional isomers can be observed from the splitting of peaks in the aromatic region. After recrystallization from MeOH/EtOAc, **1** was isolated as a white powder (13% yield). The presence of clean and sharp peaks in the ^{1}H NMR spectrum of **1** (Fig. 1b) indicate its C_5-symmetric structure. High-resolution mass spectrometry (HRMS) confirmed the formation of a pentameric product (Fig. 1c). RD-P5 **1** was further converted to RD-P5 **2** *via* a reaction with trimethylamine (Fig. 1a), maintaining its C_5-symmetric structure as confirmed by ^{1}H NMR (Fig. 1b), HRMS (Fig. 1d), and X-ray crystallography (Fig. 1e). The crystal structure of **2** showed both the expected pillar-like shape and the rim-differentiation of appended substituents. The cavity of the pillararene is occupied by disordered solvent molecules (ethanol) and one of the alkyne substituents of the rim.

The host–guest interactions between **2** and PFOS or PFOA were investigated using isothermal titration calorimetry (ITC). The binding constant K of **2** and PFOS was determined to be 2.6×10^6 M^{-1} with a P5/PFOS ratio of 1 : 5.6, analogous in strength and stoichiometry to the interactions of symmetric DAF-P5s in our previous study,[20] indicating the same binding

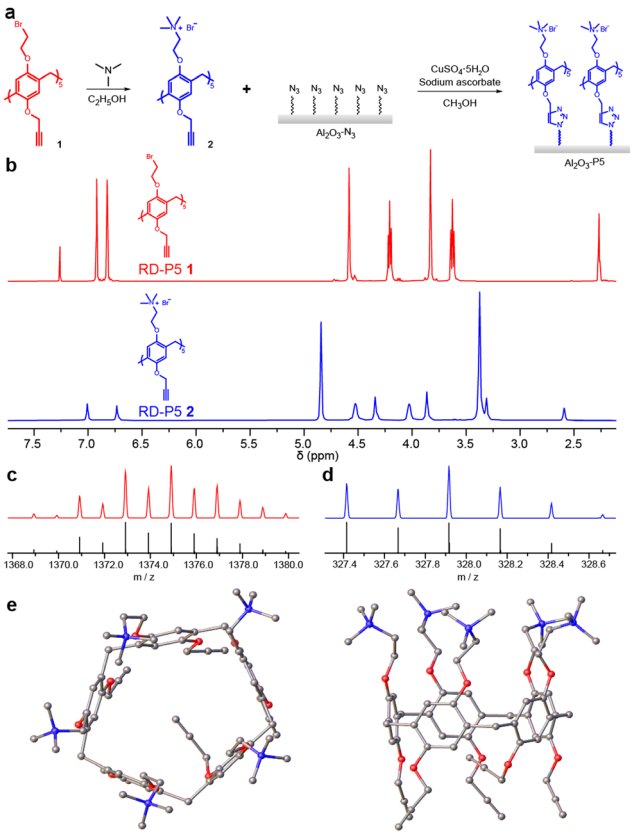

Fig. 1 (a) Synthesis of **2**-modified Al_2O_3 surface (b) ^{1}H NMR of RD-P5s **1** in $CDCl_3$ and **2** in MeOD-d_4; (c) and (d) simulated and experimental high-resolution mass spectra of RD-P5 **1** and **2**; (e) X-ray crystal structure of **2** in two orientations. Only the major component is shown. All solvent molecules, bromide counterions and hydrogen atoms have been omitted for clarity.

mode. RD-P5 **2** and PFOA display $K = 5.2 \times 10^4$ M^{-1}, with a P5/PFOA ratio of 1 : 5.9. This lower K-value is attributed to the better solubility of PFOA in water. For comparison, we also

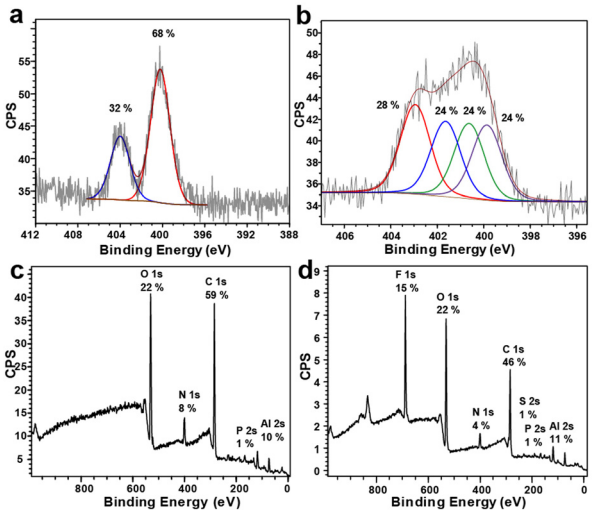

Fig. 2 XPS spectra of (a) N 1s narrow scan of Al_2O_3-N_3, (b) N 1s narrow scan of Al_2O_3-**2**, (c) survey scan of Al_2O_3-**2**, and (d) survey scan of Al_2O_3-**2**/PFOS.

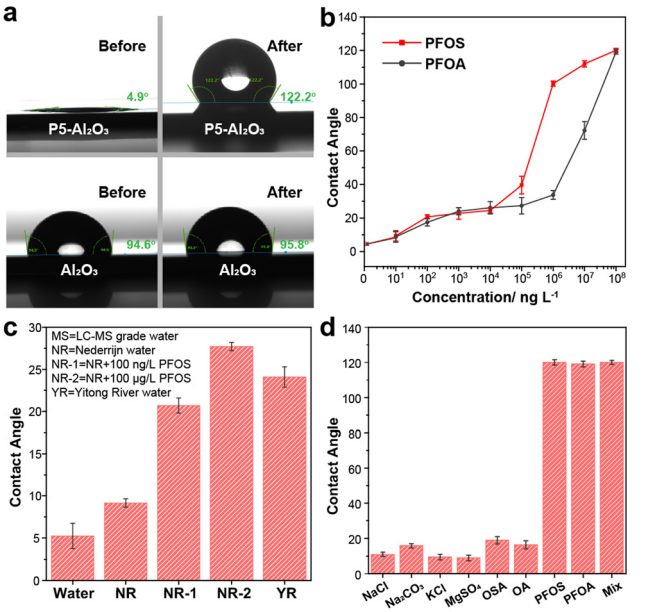

Fig. 3 (a) CA before and after immersing **2**-modified and clean Al_2O_3 surface in 100 mg L^{-1} PFOS solution; (b) CA against PFOS/PFOS concentration plot; (c) CA response of different environmental samples, PFOS/PFOA in Nederrijn (NR) is not detectable by LC-MS; total PFOS + PFOA concentration in Yitong river (YR) = 95 ng L^{-1} (LC-MS value); (d) CA response of different compounds at 100 mg L^{-1}; for the composition of mixed sample composition see main text.

tested the binding constants between **2** and octanoic acid (OA) and octanesulfonic acid (OSA), as non-fluorinated counterparts of PFOA and PFOS; no binding to either could be detected by ITC, confirming the unique involvement of the fluorous phase.[21]

In order to get a stable surface for PFAS detection, we prepared a self-assembled monolayer of 12-azidododecylphosphonic acid on an Al_2O_3 surface.[37] This was characterized using X-ray photoelectron spectroscopy (XPS), revealing two azide peaks in the N 1s narrow spectrum with the expected 2 : 1 ratio at 404.0 and 400.2 eV, respectively (Fig. 2a). RD-P5 **2** was then immobilized onto this Al_2O_3-N_3 surface using a copper(I)-catalyzed azide–alkyne cycloaddition (CuAAC) reaction. After the CuAAC reaction, the azide N 1s peak at 404.0 eV nearly completely disappeared, and it was replaced by features assigned to the triazole ring at 399.8, 400.7, 401.9 eV and a trimethylammonium group at 403.1 eV (Fig. 2b), in accordance with previous literature, indicating the successful immobilization of **2**.[37–39] Also the infrared reflection absorption spectroscopy (IRRAS) show strong decrease in the intensity of the azide peak, confirming the successful immobilization of RD-P5.

Due to the hydrophilic nature of ammonium groups, the modified Al_2O_3 surface exhibits superhydrophilicity, with a static water contact angle (CA) $<5^\circ$ (Fig. 3a). After submerging in 100 mg L^{-1} PFOS aqueous solution, the CA of the **2**-modified Al_2O_3 surface increased from 5° to 120°, indicating a transition from superhydrophilic to hydrophobic behavior. In contrast, the contact angle of a blank Al_2O_3 surface did not exhibit any significant changes upon exposure to this PFOS solution (Fig. 3a). The XPS spectrum after immersion of Al_2O_3-**2** in a 100 mg L^{-1} PFOS aqueous solution shows that the F 1s peak corresponding to PFOS has significantly increased in intensity (Fig. 3c and d), leading to a F/N ratio of 15/4. Taking into account that N 1s narrow scan shows trimethylammonium and triazole groups to be in approximately 1 : 1 ratio (Fig. 3b and Fig. S11, ESI†), and that PFOS contains 17 F atoms, the 15/4 F/N ratio means that trimethylammonium groups and PFOS are approximately in 1 : 1 ratio, or RD-P5 and PFOS ratio is around 1 : 5, suggesting a (near)-complete coverage of **2**-modified surface with PFOS. To investigate the relationship between CA and the concentration of PFOA/PFOS, a series of experiments were conducted using various concentrations of PFOA/PFOS ranging from 0 ng L^{-1} to 100 mg L^{-1}, leading to easily observable changes in CA (Fig. 3b). For PFOS, the contact angle changed from $5^\circ \pm 2^\circ$ to $10^\circ \pm 1^\circ$ after immersing into a 10 ng L^{-1} PFOS solution, showing the sensitivity to even trace amounts of PFOS. Further increases in concentration yielded a gradual increase in CA. Once the PFOS concentration exceeded 100 µg L^{-1}, the surface transitioned from hydrophilic to hydrophobic, indicating that the surface was now fully covered with a layer of PFOS. Similar trends were observed for PFOA, for which the surface became hydrophobic when the concentration of PFOA reached 10 mg L^{-1}. The higher sensitivity of **2**-modified surfaces towards PFOS compared to PFOA is fully in line with the respective binding constants measured by ITC.

One of the biggest challenges for PFOA/PFOS detection methods is their susceptibility to interference from other contaminants commonly found in nature. Factors such as pH, salt concentration, and the presence of other organic compounds can easily influence the results. To therefore further test the applicability of this method (Fig. 3c), an environmental sample was taken from the Dutch river Nederrijn (NR), which was independently confirmed to have [PFOS] $<$ 3 ng L^{-1}.[40] To this sample PFOS was added to reach concentrations of 100 ng L^{-1} (sample NR-1) and 100 µg L^{-1} (sample NR-2). The CA for NR-1 differed significantly from the original sample, showing that we can easily detect PFOS at 100 ng L^{-1} in environmental samples.

Similarly, samples from the Chinese Yitong River, with a total PFOA + PFOS concentration of 95 ng L^{-1}, showed a significantly higher CA ($24^\circ \pm 1^\circ$) than pure water samples ($5^\circ \pm 2^\circ$). In order to further demonstrate the selectivity of the Al_2O_3-**2** surface, we conducted tests with several salts commonly present in water at 100 mg L^{-1} concentration. Additionally, we tested octane sulfonic acid (OS), and octanoic acid (OA) which are non-fluorinated counterparts of PFOS and PFOA, respectively (Fig. 2d). The results clearly demonstrate the specificity towards PFOS and PFOA, as no significant increase in CA is observed in the presence of other compounds. We also prepared a ''mix'' solution containing 100 mg L^{-1} PFOS, 1 g L^{-1} NaCl, 1 g L^{-1} OA and 1 g L^{-1} OSA in one sample and showed that the CA response by PFOS is not influenced by the presence of such a mixture. In addition, simple sonication in acetone removed most of PFOS from Al_2O_3-**2** surface, allowing PFOS detection being repeated for 10 cycles (10 mg L^{-1}, see ESI† for details).

In conclusion, we have synthesized a novel rim-differentiated pillar-[5]arene (RD-P5) with dual functionality. This RD-P5 features alkyne groups on one rim for easy surface immobilization *via* various chemistries, while ammonium groups enable host–guest interactions for capturing contaminants such as PFOA and PFOS. By immobilizing RD-P5 on an aluminum oxide surface, we have demonstrated its potential application in the detection of PFOA/PFOS through contact angle measurements requiring only a modified surface and a routine smartphone. These preliminary experiments already show a robust LOD of 100 ng L^{-1}, down to 10 ng L^{-1} in some cases, thus showing significant promise for detecting PFAS-pollution in water without the need of any laboratory-based equipment. We expect such 'bringing the lab to the sample'-approaches to make important contributions to environmental monitoring efforts.

Financial support from graduate school VLAG of Wageningen University (graduate fellowship of T.-N. G.), the National Natural Science Foundation of China (grant 22011530163, to H. Z.) and Wetsus (European Centre of Excellence for Sustainable Water Technology, support to J. M. S. G.) is appreciated.

Data availability

The data supporting this article have been included as part of the ESI.†

Conflicts of interest

There are no conflicts to declare.

Notes and references

1 R. Loos, G. Locoro, S. Comero, S. Contini, D. Schwesig, F. Werres, P. Balsaa, O. Gans, S. Weiss, L. Blaha, M. Bolchi and B. M. Gawlik, *Water Res.*, 2010, **44**, 4115–4126.
2 M. Sun, E. Arevalo, M. Strynar, A. Lindstrom, M. Richardson, B. Kearns, A. Pickett, C. Smith and D. R. U. Knappe, *Environ. Sci. Technol. Lett.*, 2016, **3**, 415–419.
3 C. Lau, J. L. Butenhoff and J. M. Rogers, *Toxicol. Appl. Pharmacol.*, 2004, **198**, 231–241.
4 I. T. Cousins, R. Vestergren, Z. Wang, M. Scheringer and M. S. McLachlan, *Environ. Int.*, 2016, **94**, 331–340.
5 V. Barry, A. Winquist and K. Steenland, *Environ. Health Perspect.*, 2013, **121**, 1313–1318.
6 Y. Wang, S. B. Darling and J. Chen, *ACS Appl. Mater. Interfaces*, 2021, **13**, 60789–60814.
7 S. P. Sahu, S. Kole, C. G. Arges and M. R. Gartia, *ACS Omega*, 2022, **7**, 5001–5007.
8 S. Park, C. T. Gordon and T. M. Swager, *Proc. Natl. Acad. Sci. U. S. A.*, 2024, **121**, e2317300121.
9 R. B. Clark, D. C. Wagner, D. T. Holden, J. J. P. Roberts, E. Zumbro, L. Goodnight, K. T. Huynh, R. B. Green, J. A. Grove and J. E. Dick, *Environ. Sci. Technol.*, 2023, **57**, 21815–21822.
10 Y. H. Cheng, D. Barpaga, J. A. Soltis, V. Shutthanandan, R. Kargupta, K. S. Han, B. P. McGrail, R. K. Motkuri, S. Basuray and S. Chatterjee, *ACS Appl. Mater. Interfaces*, 2020, **12**, 10503–10514.
11 A. Concellón, J. Castro-Esteban and T. M. Swager, *J. Am. Chem. Soc.*, 2023, **145**, 11420–11430.
12 M. Zhang, Y. Zhao, B. Bui, L. Tang, J. Xue, M. Chen and W. Chen, *Crit. Rev. Anal. Chem.*, 2023, 2299233.
13 X. Chen, S. Hussain, Y. Tang, X. Chen, S. Zhang, Y. Wang, P. Zhang, R. Gao, S. Wang and Y. Hao, *Sci. Total Environ.*, 2023, **860**, 160467.
14 E. E. Harrison and M. L. Waters, *Chem. Sci.*, 2023, **14**, 928–936.
15 Q. Chen, P. Zhu, J. Xiong, L. Gao and K. Tan, *Spectrochim. Acta, Part A*, 2020, **224**, 117362.
16 A. U. Rehman, M. Crimi and S. Andreescu, *Trends Environ. Anal. Chem.*, 2023, **37**, e00198.
17 Z. Zheng, H. Yu, W. C. Geng, X. Y. Hu, Y. Y. Wang, Z. Li, Y. Wang and D. S. Guo, *Nat. Commun.*, 2019, **10**, 5762.
18 J. Zhang, Z. Wang, S. Lv, X. Zeng, Y. Sun, H. Li and R. Zhang, *Chem. Commun.*, 2019, **55**, 778–781.
19 C. Song, Z. Zhao, Y. Lin, Y. Zhao, X.-Y. Liu, C. Lin and C. Wu, *J. Colloid Interface Sci.*, 2019, **547**, 330–338.
20 T.-N. Gao, S. Huang, R. Nooijen, Y. Zhu, G. Kociok-Köhn, T. Stuerzer, G. Li, H. Bitter, G. Salentijn, B. Chen, F. M. Miloserdov and H. Zuilhof, *Angew. Chem., Int. Ed.*, 2024, e202403474.
21 L. W. Honaker, T.-N. Gao, K. R. de Graaf, T. V. M. Bogaardt, P. Vink, T. Stürzer, G. Kociok-Köhn, H. Zuilhof, F. M. Miloserdov and S. Deshpande, *Adv. Sci.*, 2024, 2401807.
22 Y. Kou, H. Tao, D. Cao, Z. Fu, D. Schollmeyer and H. Meier, *Eur. J. Org. Chem.*, 2010, 6464–6470.
23 M. Guo, X. Wang, C. Zhan, P. Demay-Drouhard, W. Li, K. Du, M. A. Olson, H. Zuilhof and A. C. H. Sue, *J. Am. Chem. Soc.*, 2018, **140**, 74–77.
24 P. Demay-Drouhard, K. Du, K. Samanta, X. Wan, W. Yang, R. Srinivasan, A. C. H. Sue and H. Zuilhof, *Org. Lett.*, 2019, **21**, 3976–3980.
25 G. Yu, Y. Ma, C. Han, Y. Yao, G. Tang, Z. Mao, C. Gao and F. Huang, *J. Am. Chem. Soc.*, 2013, **135**, 10310–10313.
26 Y. Yao, M. Xue, Z. Zhang, M. Zhang, Y. Wang and F. Huang, *Chem. Sci.*, 2013, **4**, 3667–3672.
27 G. Yu, Z. Zhang, C. Han, M. Xue, Q. Zhou and F. Huang, *Chem. Commun.*, 2012, **48**, 2958–2960.
28 H. Zhang, X. Ma, K. T. Nguyen and Y. Zhao, *ACS Nano*, 2013, **7**, 7853–7863.
29 P. Liu, Y. Deng, J. Lu, X. Gou, Q. Han, Y.-R. Pei and L. Y. Jin, *Polym. Int.*, 2023, **73**, 359–367.
30 R. Chang, C.-Y. Chen, L. Gao, Y. Li, Z.-H. Lee, H. Zhao, A. C. H. Sue and K.-C. Chang, *Org. Biomol. Chem.*, 2024, **22**, 745–752.
31 W. Yang, K. Samanta, X. Wan, T. U. Thikekar, Y. Chao, S. Li, K. Du, J. Xu, Y. Gao, H. Zuilhof and A. C.-H. Sue, *Angew. Chem., Int. Ed.*, 2020, **59**, 3994–3999.
32 L. Luo, G. Nie, D. Tian, H. Deng, L. Jiang and H. Li, *Angew. Chem., Int. Ed.*, 2016, **55**, 12713–12716.
33 J. Lu, P. Liu, Y. Deng, N. Zhu and L. Y. Jin, *J. Mol. Struct.*, 2023, **1291**, 136054.
34 B. Lu, X. Yan, J. Wang, D. Jing, J. Bei, Y. Cai and Y. Yao, *Chem. Commun.*, 2022, **58**, 2480–2483.
35 Z. Liu, F. Demontrond, A. Imberty, A. C. H. Sue, S. Vidal and H. Zhao, *Chin. Chem. Lett.*, 2023, **34**, 107872.
36 J. Zhao, W. Yang, C. Liang, L. Gao, J. Xu, A. C. H. Sue and H. Zhao, *Chem. Commun.*, 2021, **57**, 11193–11196.
37 A. Debrassi, E. Roeven, S. Thijssen, L. Scheres, W. M. de Vos, T. Wennekes and H. Zuilhof, *Langmuir*, 2015, **31**, 5633–5644.
38 A. R. Kuzmyn, L. W. Teunissen, M. V. Kroese, J. Kant, S. Venema and H. Zuilhof, *ACS Omega*, 2022, **7**, 38371–38379.
39 J. Zhao, F. Gao, S. P. Pujari, H. Zuilhof and A. V. Teplyakov, *Langmuir*, 2017, **33**, 10792–10799.
40 W. A. Gebbink, L. van Asseldonk and S. P. J. van Leeuwen, *Environ. Sci. Technol.*, 2017, **51**, 11057–11065.

